*Eur. J. Biochem.* **269**, 3894–3904 (2002) © FEBS 2002 doi:10.1046/j.1432-1033.2002.03055.x

# Schemes of flux control in a model of *Saccharomyces cerevisiae* glycolysis

**Leighton Pritchard and Douglas B. Kell**

*Institute of Biological Sciences, University of Wales, Aberystwyth, UK*

We used parameter scanning to emulate changes to the limiting rate for steps in a fitted model of glucose-derepressed yeast glycolysis. Three flux-control regimes were observed, two of which were under the dominant control of hexose transport, in accordance with various experimental studies and other model predictions. A third control regime in which phosphofructokinase exerted dominant glycolytic flux control was also found, but it appeared to be physiologically unreachable by this model, and all realistically obtainable flux control regimes featured hexose transport as a step involving high flux control.

*Keywords*: yeast; metabolic control analysis; glycolysis; modelling; flux.

*In vivo* and *in vitro* investigations of metabolic pathways can be complex and expensive. The need to focus efficiently both monetary and physical effort necessitates that some pathways and organisms will be only partially explored by experiment, while others will be neglected completely. Bioinformatic and computational approaches offer a means of obtaining full value from experimentally acquired data, extending their interpretation, suggesting novel hypotheses for future experiments and guiding the experimentalist towards potentially rewarding investigations but away from likely fruitless ones. In this paper, we use such an approach, parameter scanning, to investigate the operation of a model of glucose derepressed yeast glycolysis (fitted by evolutionary computing to experimental data) under a far wider range of conditions than could be considered *in vitro* or *in vivo*, which suggests opportunities for further experiment.

Glycolysis is perhaps the most important pathway in the metabolism of many living cells, describing the conversion of glucose (and sometimes other hexoses) to pyruvate and thence, in some organisms, to ethanol. In this conversion two molecules of ATP are consumed and four molecules of ATP are generated, providing a major source of 'negotiable energy' for the cell. The glycolytic pathway, though crucial to each, varies in detail between organisms [1]; for largely economic reasons, greater effort has gone into the understanding of glycolysis in some organisms than in others. Brewer's yeast *Saccharomyces cerevisiae*, and in particular its glycolytic pathway, is of great economic importance, not least for the production of ethanol in the brewing and distilling industries. The study of yeast glycolysis has thus been the focus of scientific interest for over a century. In pregenomic studies, the enzymes and metabolites that make up the pathway were considered to have been elucidated completely [2], but the solution of the *S. cerevisiae* genome added further to this knowledge, and it is widely considered that this organism currently possesses the best-investigated and best-understood glycolytic pathway.

Much effort has already been invested in mathematical modelling of the glycolytic pathway in yeast [3–8] and in other organisms, such as *Trypanosoma brucei*, the parasite that causes sleeping sickness [9–12]. The success and utility of modelling in the study of *T. brucei* glycolysis has even led to the coining of a new strategy for the investigation of metabolism: computer experimentation [11]. This is intended to be a substitute for practical experimentation, and must be based on precise kinetic knowledge of the system. For yeast glycolysis, the most complete model to date was constructed in order to test whether combining the properties of the individual enzymes in isolation would yield a proper description of the pathway as a whole [7]. This work provided a unique and highly valuable set of *in vitro* kinetic and physical data obtained under a consistent set of conditions (rare in the field [13]), and represented a major step towards such computer experimentation in yeast.

In this paper, and in the spirit of computer experimentation, we use the parameter scanning functions of GEPASI [14–16] to generate over 8000 models of glucose-derepressed yeast glycolysis in order to test the flux-control characteristics of the Teusink *et al.* model [7] under a wide range of enzyme limiting rates. The limiting rates for 13 steps of the model were scanned independently in all combinations by an overall factor of four. In this way we explore the flux-control behaviour of the model within the limits of its

*Correspondence to* D. B. Kell, Cledwyn Building, Institute of Biological Sciences, University of Wales, Aberystwyth, Wales, UK, SY23 3DD.
Fax: + 44 1970622354, Tel.: + 44 1970622334,
E-mail: dbk@aber.ac.uk

*Abbreviations*: PCA, principal components analysis; $C^J_X$, flux control coefficient for step X and flux J; FCC, flux control coefficient; Glyc, glycogen branch; Succ, succinate branch; Treh, trehalose branch.

*Enzymes*: alcohol dehydrogenase (EC 1.1.1.1); adenylate kinase (EC 2.7.4.2); aldolase (EC 4.1.2.13); enolase (EC 4.2.1.11); glycerol-3-phosphate dehydrogenase (EC 1.1.99.5); glyceraldehyde-3-phosphate dehydrogenase (EC 1.2.1.12); hexokinase (EC 2.7.1.1); pyruvate decarboxylase (EC 4.1.1.1); phosphofructokinase (EC 2.7.1.11); phosphoglucoisomerase (EC 5.3.1.9); phosphoglycerate kinase (EC 2.7.2.3); phosphoglycerate mutase (EC 5.4.2.1); pyruvate kinase (EC 2.7.1.40); triosephosphate isomerase (EC 5.3.1.1).

*Note*: a web site is available at http://qbab.dbs.aber.ac.uk

(Received 24 January 2002, revised 10 June 2002, accepted 18 June 2002)

description of glucose-derepressed glycolysis and fixed fluxes to glycogen and trehalose.

Although the *in vitro* kinetic data from [7] are rather precise and quite complete, the generated model was unable perfectly to describe the system's *in vivo* behaviour. The authors, however, were not aiming to give the best possible description of the experimental system, but were instead investigating whether the isolated, *in vitro* kinetics of the glycolytic enzymes could describe the experimental system. Nonetheless they attempted to fit individual steps to experimental data, but restrained themselves from attempting to fit simultaneously the whole model, and from presuming that the intracellular concentration of enzyme was the single cause of the discrepancy between *in vitro* and *in vivo* behaviour for each individual step; they also considered the effects of altered substrate/product affinities and equilibrium constants. It was seen that, for most of the enzymes, only a small change in the value of the limiting rate was required for *in silico* kinetics to match each individual enzyme's *in vivo* performance closely. While modifications of $V_{max}$ alone to fit *in vivo* performance could be calculated analytically for most steps in glycolysis, this was not the case for all steps [7].

In this paper, we use a version of the model of glucose-derepressed wild type yeast glycolysis described in [7] and investigate characteristics of its operation close to the wild-type state, and over a much wider range of operation than that for which the model was originally intended. It has been suggested [17] that inductive, multivariate and machine learning approaches are appropriate for such problems, and so we used the evolutionary programming algorithms incorporated in the metabolic modelling package GEPASI [14–16] to estimate multiple sets of $V_{max}$ values for the glycolytic enzymes that enable the model to describe *in vivo* behaviour closely. Such an approach, although unlike algebraic analysis in that it produces a range of possible (although inexact) fits to the data, accounts for the effect of simultaneously varying the kinetics of the other steps, and is also expected to be a better qualitative measure of the flexibility of the model itself in describing the experimental data than is algebraically fitting isolated steps to their *in vivo* performance. As a population operating approximately equally close to the observed experimental state in [7], these models may be considered to represent natural variability in the yeast population, and we investigated the regions of parameter and variable space described by them. Metabolic control analysis [18–21] was performed on the fitted models, and rank correlation analysis [22,23] used to investigate patterns of flux control. The model with the best-fit $V_{max}$ parameters was used as the base model for parameter scanning using routines contained in GEPASI.

## METHODS

### Model

A model of branched glycolysis, as described in [7] was obtained in SCAMP format from one of its authors (a kind gift from B. Teusink, TNO Prevention and Health, Leiden, the Netherlands.) and is illustrated schematically in Fig. 1. The ordinary differential equations describing the model are

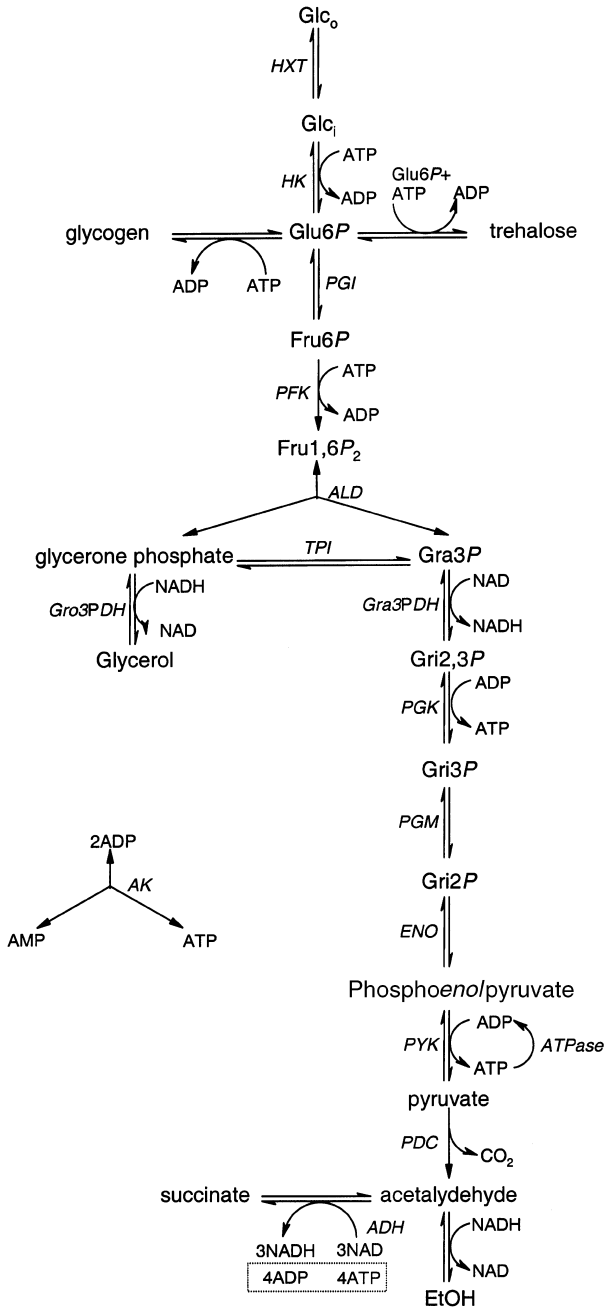


**Fig. 1. Schematic of the model yeast glycolytic pathway.** The boxed areas indicate the 'perturbation' of including ATP/ADP conversion in the succinate step which was present in [7], but not the provided SCAMP model. The ATP-ADP conversion is not included in the GEPASI model described herein. AMP, adenosine monophosphate; EtOH, ethanol; Fru1,6$P_2$, fructose 1,6-biphosphate; Fru6*P*, fructose 6-phosphate; GLCi, glucose (internal); GLCo, glucose (external); Gri3*P*, 3-phosphoglycerate; Gri3*P*, 2-phosphoglycerate; Gri1,3$P_2$, 1,3-bisphosphoglycerate; ADH, alcohol dehydrogenase; AK, adenylate kinase; ALD, aldolase; ENO, enolase; Gro3*P*DH, glycerol-3-phosphate dehydrogenase; Glc6*P*, glucose-6-phosphate; Gra3*P*, D-glyceraldehyde-3-phosphate; Gra3*P*DH, glyceraldehyde-3-phosphate dehydrogenase; HK, hexokinase; HXT, hexose transport; PDC, pyruvate decarboxylase; PFK; phosphofructokinase; PGI, phosphoglucoisomerase; PGK, phosphoglycerate kinase; PGM, phosphoglycerate mutase; PYK, pyruvate kinase; TPI, triosephosphate isomerase.

given in appendix 1. The SCAMP file was converted manually to GEPASI [14] format, requiring minor modifications, and is available to download from http://users.aber.ac.uk/lep/models.shtml. Another version of the model may be run via the internet at http://jjj.biochem.sun.ac.za. The variant of the model upon which we base our work contains small deviations (described in Appendix 2) from that published in [7], but with the exception of steady-state pyruvate concentration, behaves identically to the published model.

### Statistical methods and parameter fitting

Student's *t*-tests and Spearman's rank correlation analysis were performed as described in [22,23] and using tables therein. Principal components analysis (PCA) [24–26] was performed using HOBBES, an in-house multivariate statistics package [27,28]. Parameter fitting was performed on the model using the evolutionary programming (genetic) algorithm incorporated in GEPASI [16], with a population of 50 models running for 300 generations. We fitted $V_{max}$ values for all steps (simultaneously constrained between 1 and $10^4$ units) to the experimentally determined steady-state mean metabolite concentrations using a sum of squares difference cost function. Independent fitting runs were performed on a number of generic PC clones under WINDOWS 95/NT.

## RESULTS

### Comparison of fitted $V_{max}$ values with those obtained by experiment

Fitted $V_{max}$ values from 10 fitting runs of 300 generations with a population of 50 models, and the corresponding steady-state metabolite concentrations and fluxes, are shown in Tables 1 and 2. The fitted $V_{max}$ values occupy only a very small portion of the available parameter space, close to those obtained experimentally *in vitro* in [7]. PCA and two-tailed *t*-tests indicate that the fitted model values cluster loosely together with the experimentally determined $V_{max}$ values, and that only six of the 14 $V_{max}$ values are significantly altered in fitting ($P < 0.05$). Altered $V_{max}$ values are found in two contiguous sections of the pathway, one in upper glycolysis (PGI-PFK-ALD; see Fig. 1 for definitions of metabolites and enzymes) and one in lower glycolysis (ENO-PYK-PDC), and the required adjustments correspond, not unexpectedly, to those determined in [7].

The steady-state metabolite concentrations from the fitted models are much closer to the experimentally determined values than are those from the original model (Table 2). Although fitting the glycolysis model to the experimental data radically improves its performance, PCA shows that the distribution of these modelled concentrations is still not congruent with the *in vivo* values (Fig. 2B), but that this variation is, however, negligible compared to the difference between the original and fitted model values (Table 3). The steady-state fluxes of the original model lie well within the range covered by the steady-state fluxes of the fitted models, which are distinct from the *in vivo* steady-state fluxes (Fig. 2C).

Three replicate measurements of *in vivo* metabolite concentration and pathway flux were made in [7], permitting statistical comparison of the fitted and experimental steady-state metabolite concentrations and pathway fluxes. Student's *t*-tests showed that three of 15 (Fru6*P*, glycerone phosphate, phospho*enol*pyruvate) metabolite concentration and two HXTs, (lower glycolysis) of five flux value populations differed significantly between the fitted and experimental values ($P < 0.05$). Although the fitting procedure improved the performance of the model markedly in terms of its ability to predict individual metabolite concentrations and fluxes, it did not produce an exact match for the measured *in vivo* behaviour.

### Flux-control coefficients are uniform across all fitted models

Mean values for each flux control coefficient (FCC), the corresponding sample standard deviations and coefficients of variation (CoV) across all fitted models were calculated. The standard deviations of the FCCs for steps with

**Table 1. $V_{max}$ values for fitted models.** Values of $V_{max}$ obtained for each fitted step of the glycolysis model in each of the 10 fitting runs, and the means and standard deviations of this population for each step.

| | Run | | | | | | | | | | | |
|---|---|---|---|---|---|---|---|---|---|---|---|---|
| Step | R1 | R2 | R3 | R4 | R5 | R6 | R7 | R8 | R9 | R10 | Mean | SD |
| HXT | 97.24 | 96.82 | 94.78 | 81.05 | 114.5 | 96.02 | 98.23 | 93.28 | 98.39 | 98.75 | 96.91 | 8.08 |
| HK | 236.7 | 295.2 | 323.9 | 243.1 | 195.2 | 200.7 | 227.8 | 214.6 | 258.5 | 231.6 | 242.8 | 40.54 |
| PGI | 1056 | 656.9 | 705.9 | 362.7 | 1125 | 1318 | 334.3 | 313.1 | 1331 | 1560 | 876.3 | 461.3 |
| PFK | 110.0 | 122.1 | 119.0 | 112.6 | 129.4 | 108.0 | 154.6 | 154.9 | 114.5 | 110.8 | 123.6 | 17.62 |
| ALD | 94.69 | 95.66 | 92.56 | 80.36 | 103.8 | 88.00 | 92.76 | 87.46 | 93.32 | 92.19 | 92.08 | 6.10 |
| Gra3*P*DH(f) | 1152 | 1078 | 1162 | 1161 | 1168 | 1267 | 1167 | 1268 | 1221 | 1288 | 1193 | 65.91 |
| Gra3*P*DH(r) | 6719 | 6504 | 6481 | 5642 | 6551 | 6687 | 6437 | 6548 | 6294 | 6530 | 6439 | 304.6 |
| Gro3*P*DH | 47.11 | 69.66 | 64.29 | 9.83 | 109.4 | 42.22 | 62.02 | 33.10 | 72.84 | 57.92 | 56.84 | 26.56 |
| PGK | 1288 | 1178 | 1498 | 1600 | 1399 | 1344 | 1369 | 1256 | 1287 | 1161 | 1338 | 136.5 |
| PGM | 2585 | 2349 | 2410 | 2956 | 2131 | 2517 | 2645 | 1105 | 2478 | 2635 | 2381 | 497.4 |
| ENO | 201.6 | 209.4 | 204.7 | 182.5 | 222.3 | 198.1 | 206.7 | 221.5 | 203.9 | 205.9 | 205.7 | 11.34 |
| PYK | 1000 | 946.7 | 943.2 | 1053 | 1094 | 1068 | 884.2 | 1089 | 1114 | 1069 | 1026 | 77.89 |
| PDC | 857.8 | 867.8 | 864.2 | 710.0 | 897.5 | 833.3 | 827.2 | 814.0 | 634.9 | 878.1 | 818.5 | 82.77 |
| ADH | 209.5 | 737.6 | 824.9 | 781.5 | 824.1 | 742.3 | 826.8 | 770.6 | 849.4 | 371.7 | 693.9 | 219.1 |

**Table 2. Steady-state metabolite concentrations and fluxes for fitted models.** The values of steady-state metabolite concentrations (mM) and pathway fluxes (mM·min$^{-1}$) obtained in each of the 10 fitting runs, and similar values for the same model run using experimentally obtained $V_{max}$ parameters from [7]. The sum of squares difference used as a cost function is also indicated, with an estimate made for the sum of squares difference between the original model and experimental metabolite concentrations. Note that fitting does not significantly alter the fluxes. SSQ, sum of squares.

| | Fitting run | | | | | | | | | | |
|---|---|---|---|---|---|---|---|---|---|---|---|
| Metabolite | R1 | R2 | R3 | R4 | R5 | R6 | R7 | R8 | R9 | R10 | Teusink Model |
| [ATP] | 2.48 | 2.54 | 2.56 | 2.52 | 2.63 | 2.61 | 2.58 | 2.65 | 2.58 | 2.56 | 2.51 |
| [Glc6*P*] | 2.44 | 2.53 | 2.52 | 2.45 | 2.50 | 2.46 | 2.62 | 2.61 | 2.44 | 2.44 | 1.07 |
| [ADP] | 1.31 | 1.27 | 1.26 | 1.28 | 1.22 | 1.23 | 1.25 | 1.21 | 1.25 | 1.26 | 1.29 |
| [Fru6*P*] | 0.57 | 0.51 | 0.53 | 0.41 | 0.58 | 0.60 | 0.37 | 0.37 | 0.59 | 0.61 | 0.11 |
| [Fru1,6$P_2$] | 5.52 | 5.61 | 5.51 | 5.47 | 5.52 | 5.47 | 5.49 | 5.47 | 5.53 | 5.49 | 0.61 |
| [AMP] | 0.31 | 0.29 | 0.28 | 0.29 | 0.25 | 0.26 | 0.27 | 0.25 | 0.27 | 0.28 | 0.30 |
| [glycerone phosphate] | 0.97 | 0.94 | 0.86 | 1.03 | 0.89 | 0.82 | 0.86 | 0.86 | 0.82 | 0.81 | 0.74 |
| [Gra3*P*] | 0.04 | 0.04 | 0.04 | 0.05 | 0.04 | 0.04 | 0.04 | 0.04 | 0.04 | 0.04 | 0.03 |
| [NAD] | 1.50 | 1.55 | 1.54 | 1.42 | 1.56 | 1.53 | 1.54 | 1.52 | 1.55 | 1.53 | 1.55 |
| [NADH] | 0.09 | 0.04 | 0.05 | 0.17 | 0.03 | 0.06 | 0.05 | 0.07 | 0.04 | 0.06 | 0.04 |
| [Gri3*P*] | 0.84 | 0.87 | 0.90 | 0.77 | 0.91 | 0.88 | 0.90 | 0.92 | 0.89 | 0.83 | 0.36 |
| [Gri2*P*] | 0.12 | 0.12 | 0.13 | 0.12 | 0.12 | 0.13 | 0.13 | 0.09 | 0.13 | 0.12 | 0.04 |
| [pyrauvate] | 1.80 | 1.81 | 1.81 | 1.91 | 1.85 | 1.83 | 1.86 | 1.86 | 2.23 | 1.80 | 8.37 |
| [acetaldehyde] | 0.18 | 0.18 | 0.17 | 0.05 | 0.24 | 0.13 | 0.16 | 0.11 | 0.18 | 0.17 | 0.17 |
| **Flux** | | | | | | | | | | | |
| Glucose | 88.27 | 90.08 | 88.83 | 75.23 | 97.58 | 85.59 | 88.83 | 84.44 | 90.34 | 89.42 | 88.15 |
| Ethanol | 128.56 | 131.33 | 131.14 | 121.83 | 138.28 | 130.59 | 131.68 | 130.83 | 132.48 | 131.37 | 129.23 |
| CO2 | 136.10 | 139.07 | 138.26 | 123.84 | 148.36 | 136.01 | 138.65 | 135.53 | 140.08 | 138.76 | 136.50 |
| Glycerol | 18.85 | 19.35 | 17.80 | 5.02 | 25.20 | 13.56 | 17.42 | 11.75 | 19.00 | 18.49 | 18.19 |
| Succinate | 3.77 | 3.87 | 3.56 | 1.00 | 5.04 | 2.71 | 3.48 | 2.35 | 3.80 | 3.70 | 3.64 |
| **SSQ** | 0.031 | 0.038 | 0.036 | 0.035 | 0.040 | 0.033 | 0.043 | 0.042 | 0.041 | 0.033 | > 36 |

significant flux control coefficients were uniformly close to zero. Several CoVs approach a value of one, but only where the flux control coefficient is negligibly small.

For steps in main-chain glycolysis, with few exceptions, the only significant glycolytic flux control derives from the hexose transport ($C^J_{HXT} \approx 1$) and hexokinase ($C^J_{HK} \approx 0.15$) steps, though there is frequently small negative flux control from ATPase and the glycogen/trehalose branching steps ($C^J_{ATPase} \approx -0.08$; $C^J_{Glyc} \approx -0.09$; $C^J_{Treh} \approx -0.07$). The remaining steps of glycolysis exert only minimal, but exclusively positive flux control over the main-chain glycolytic steps, and the sum of glycolytic flux control coefficients for these steps is approximately 0.1 for any given flux.

Control over ATPase flux which, in this model, represents generalized ATP use (or demand) in the organism, follows a similar pattern to that for main-chain glycolysis, in that flux control rests with the HXT ($C^{ATPase}_{HXT} \approx 1.4$) and HK ($C^{ATPase}_{HK} \approx 0.2$) steps. Again, the branching steps also exert some negative flux control and main-chain glycolytic enzymes exert only slightly greater control over ATPase than they do over the main glycolytic flux.

In our simulations, the fluxes through the glycogen and trehalose branches are fixed, as we use the Teusink *et al.* model [7], simulating only glucose derepressed glycolysis. Only the Gro3*P*DH (leading to glycerol) and succinate branches are subject to flux control by other steps, and the FCCs are identical in each branch. These two branches, and the subsections of metabolism that they represent, have some autonomous control over their own steady-state flux in this model. The major FCC is again that of hexose transport ($C^J_{HXT} \approx 0.72$), but there are also two large positive FCCs from the Gro3*P*DH ($C^{Gro3PDH,succ}_{Gro3PDH} \approx 0.56$) and succinate ($C^{Gro3PDH,succ}_{Succ} \approx 0.33$) branches themselves. The hexokinase step also has a positive influence on pathway flux ($C^{Gro3PDH,succ}_{HK} \approx 0.11$), and the steps of lower glycolysis exert significant negative flux control ($C^{Gro3PDH,succ}_{Gra3PDH} \approx -0.19$; $C^{Gro3PDH,succ}_{ADH} \approx -0.13$). A precise division between upper and lower glycolysis can be made, in that upper glycolytic enzymes (HK-ALD) have positive FCCs and lower glycolytic enzymes (steps Gra*3*PDH-ADH) have negative FCCs for the succinate and glycerol branching steps.

## Correlation analysis of control coefficients

We used the nonparametric method of Spearman's rank correlation analysis [22,23], coded in-house, to detect statistically significant correlations between the magnitudes of the FCCs across the fitted glycolysis models and thus identify patterns of distributed control in this system (Fig. 3A–D). Overall, the correlation between the FCCs $C^J_x$ and $C^J_y$ for all pairs of enzymes ($x$, $y$) over all steps J is of constant sign where the FCC and correlation are significant. This implies strong linkage of the controlling behaviour of groups of steps in glycolysis. Where FCCs for branching steps are significantly correlated with each other, this correlation is always positive, and where FCCs for the main-chain of glycolysis (HK-ADH) are correlated with each other, these, too are also positive. The FCCs for branching steps are negatively correlated with those for main-chain glycolysis, and there is also a negative correlation between FCCs for HXT and the rest of main-chain glycolysis.

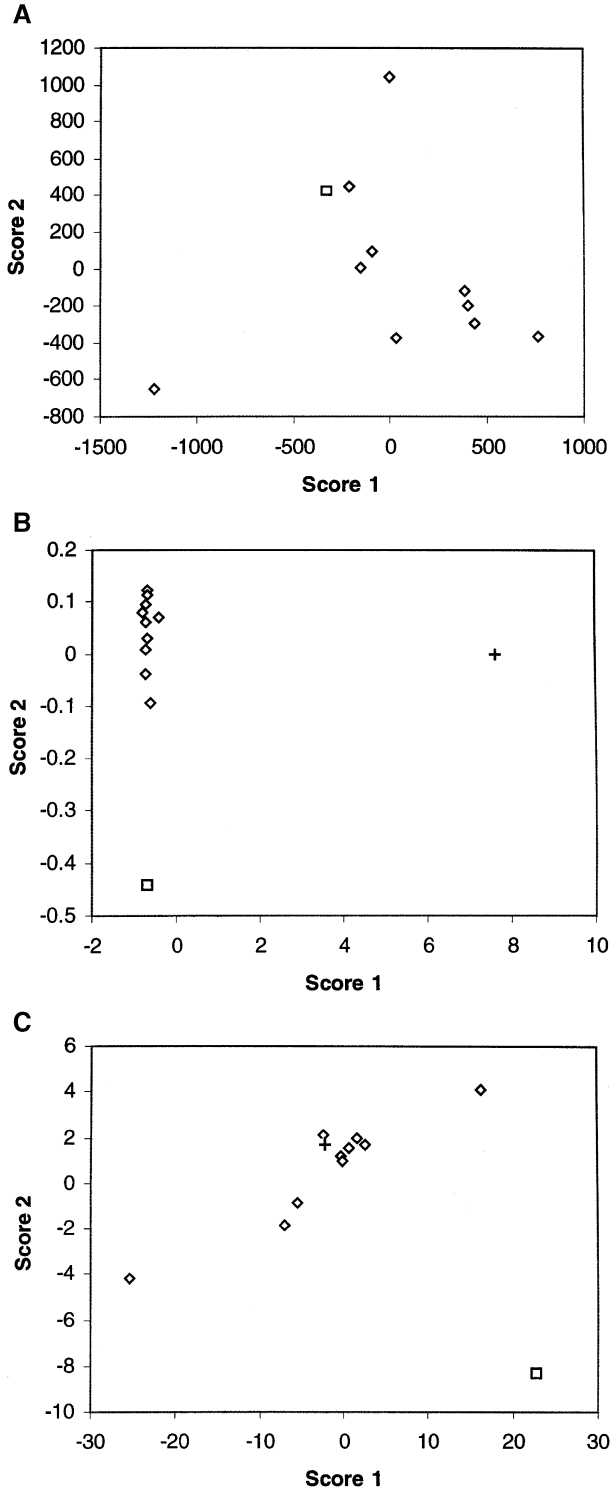


**Fig. 2. PCA score plots for: (A) model $V_{max}$ values from fitting (diamonds) and experiment (squares), (B) steady-state metabolite concentration values from fitting (diamonds), *in vivo* studies (square) and the original model (cross), and (cB) steady-state fluxes from fitting (diamonds), *in vivo* studies (square) and the original model (cross). Experimental data from [7].** (A) The experimental values lie on the outskirts of the main fitted cluster, and the main outlier is a fitted model, indicating that the adjustments made to $V_{max}$ values to fit the experimental data need not be great, largely cluster together, and form a different distribution to the experimentally determined values. (B) Score 1 explains over 99% of the total variance, so the gulf between the results of the original model and the set of fitted and experimental concentrations is much greater than that which separates the fitted and experimental concentrations themselves. The clustering of fitted models indicates that the fit of metabolite concentrations to the *in vivo* values, though much better than the original model, is still not exact. (C) The fitted values can be viewed either as a continuum between two extremes, or as a cluster with two outliers. By either interpretation the fluxes described by the original model are contained within the distribution of fitted models. The *in vivo* fluxes, however, are clear outliers to this distribution. This plot suggests that the model as described in [7] and herein, is not capable of representing the state of glycolysis determined experimentally in the Teusink *et al.* paper.

## Parameter scanning

The manner in which control of glycolytic flux changes when expression levels of glycolytic enzymes are altered was investigated by independently varying $V_{max}$ values for HXT, HK, PGI, PFK, ALD, Gra3*P*DH (forward and reverse) PGK, PGM, ENO, PYK, PDC, and ADH by an overall factor of four (limiting rates were set to either $V_{max}/2$ or $2V_{max}$ in all combinations) using the parameter scanning functions of GEPASI. Only around 50% of the simulations reached steady state, and of those that did a single step was usually seen to dominate flux control (Fig. 4A,B).

No steady state was reached in which a high limiting rate of HXT (200 μmol·mL$^{-1}$·min$^{-1}$) was accompanied by either a low rate for HK(50 μmol·mL$^{-1}$·min$^{-1}$) or a high one for PFK (240 μmol·mL$^{-1}$·min$^{-1}$). The ability of the scanned systems to reach steady state could be described by two simple rules. All systems were able to reach steady state with low HXT limiting rate (50 μmol·mL$^{-1}$·min$^{-1}$) unless HK, Gra3*P*DH (forward) and ADH limiting rates were reduced (to 200, 1700 and 25 μmol·mL$^{-1}$·min$^{-1}$, respectively). Conversely, those systems with large HXT($V_{max}$) could only reach steady-state if the limiting rates for HK, PFK and ALD were low (200, 60 and 50 μmol·mL$^{-1}$·min$^{-1}$, respectively). 3584 systems with high HXT limiting rate could not therefore reach steady-state, compared to only 512 with low HXT($V_{max}$).

PCA of the FCCs for those simulations able to attain steady state indicates that within the scanned parameter range this model of derepressed glycolysis operates under one of three major modes of control (Figs 4 and 5). In regimes II and III, HXT is the step dominating glycolytic flux control, and the only other step seen to dominate glycolytic flux control is PFK in regime I. Dominant PFK flux control is limited to a small region of parameter space in which its limiting rate is halved, while HXT($V_{max}$) is doubled. More detailed scanning (50 μmol·mL$^{-1}$·min$^{-1}$ < PFK, HXT($V_{max}$) < 200 μmol·mL$^{-1}$·min$^{-1}$ in 15 μmol·mL$^{-1}$·min$^{-1}$ steps) of this parameter region illustrates the boundary between the two control regimes (Fig. 6). As the model moves into the PFK flux control region internal concentrations of G6P and Fru6*P* rapidly rise to pathological levels (Fig. 6), suggesting that this state may not be physiologically accessible under the conditions of this model, in which the flux to glycogen and trehalose is fixed.

The regime occupied most frequently by our simulations is regime II, wherein glycolytic flux control is almost exclusively the province of hexose transport, with minor

**Table 3. Eigenvalues from PCA of fitted models.** Eigenvalues, and the percentage of total variance explained by each eigenvalue, for the first five principal components in PCA of the fitted $V_{max}$ values, steady-state glycolytic fluxes and steady-state metabolite concentrations of the fitted models and the corresponding experimentally derived values. Most variance is explained in the first two principal components (PCs) in each case.

| | $V_{max}$ | | Flux | | Metabolite conc | |
|---|---|---|---|---|---|---|
| PC | Abs | % | Abs | % | Abs | % |
| 1.00 | $2.77 \times 10^6$ | 42.49 | 1525.74 | 90.73 | 63.08 | 99.10 |
| 2.00 | $2.31 \times 10^6$ | 35.38 | 125.51 | 7.46 | 0.26 | 0.41 |
| 3.00 | $6.24 \times 10^5$ | 9.57 | 30.40 | 1.81 | 0.13 | 0.21 |
| 4.00 | $4.44 \times 10^5$ | 6.81 | 0.00 | 0.00 | 0.08 | 0.13 |
| 5.00 | $2.54 \times 10^5$ | 3.90 | 0.00 | 0.00 | 0.06 | 0.10 |
| Total | $6.52 \times 10^6$ | | 1681.65 | | 63.65 | |

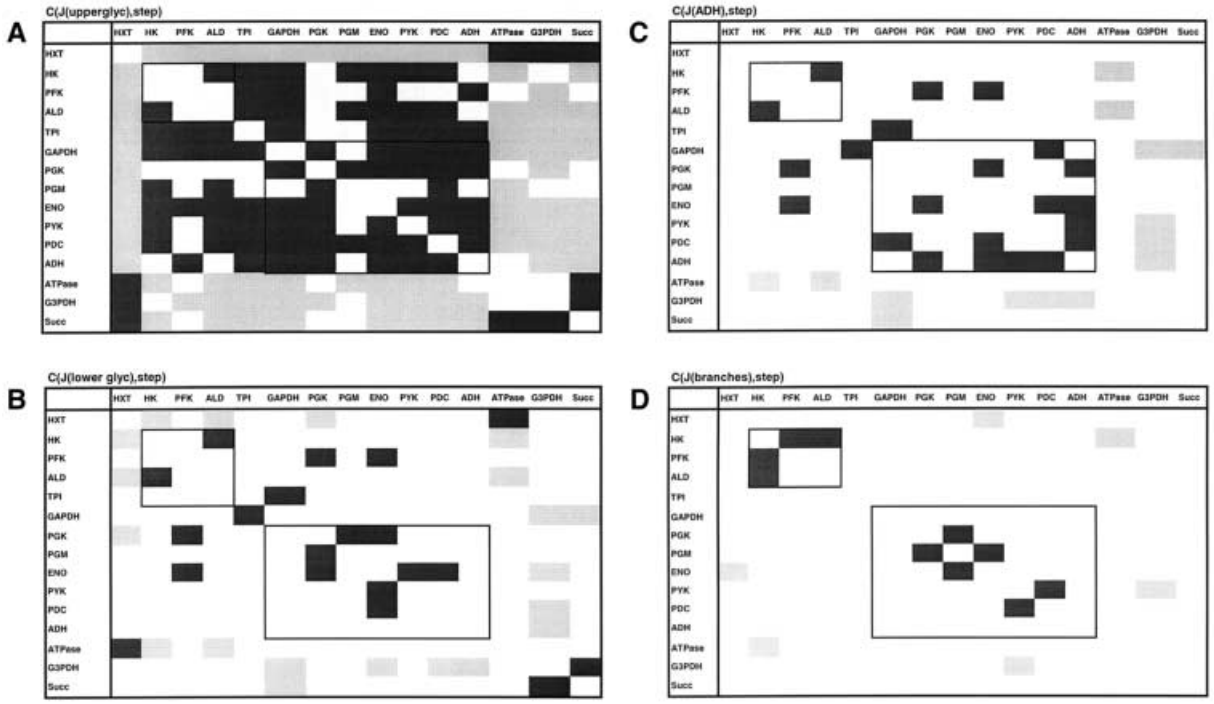


**Fig. 3. Significant correlations (two-tailed Spearman's Rank, $P < 0.05$) between flux control coefficients for glycolytic fluxes across all fitted models.** Positive correlations are indicated by heavy shading, negative by light shading. The sets of fluxes are grouped into (A) upper glycolysis (PGI, PFK, ALD), (B) lower glycolysis (Gra3*P*DH-PDC), (C) ADH, and (D) succinate and glycerol branches.

contributions from hexokinase in the circumstances that both HXT and HK $V_{max}$ values are halved, and ADH($V_{max}$) is doubled. Regime III features significant joint glycolytic flux control by HXT, HK and ADH. This regime is characterized by low ADH($V_{max}$) and high Gra3*P*DH($V_{max}$) and is similar to a sub regime of extreme PFK flux control in which $C_{ADH}^{J(glycolysis)}$ approaches 0.2, in that it is correlated with reduced ADH($V_{max}$) and that an exponential increase in FCCs is seen (Figs 4 and 5). Each of the three major flux control regimes contains several sub regimes, but the gross features of each remain as stated.

## DISCUSSION

### Model fitting

The original fitting procedure employed in [7] algebraically fitted the $V_{max}$ values for individual steps to experimentally determined mean metabolite concentrations and pathway fluxes. With such mathematical precision available, it may be argued that the computationally expensive stochastic fitting procedure we employed is unnecessary. However, individual algebraic fitting of the model steps has the advantage of providing exact solutions only with this caveat: that the solutions so found fit exactly to mean experimental values, which themselves contain some uncertainty. Each such solution represents only one possible experimental state that may not actually have been observed. Multiple fits for individual steps compound this problem, and may produce the illusion of an absolute and unambiguous fit of the whole model to experimental data where this is not, in fact, the case. Indeed, in [7] an exact fit proved not to be possible for all model steps within the constraints of the Haldane equation, so the model as a whole could not be fit absolutely to the experimentally determined means. For this work, we

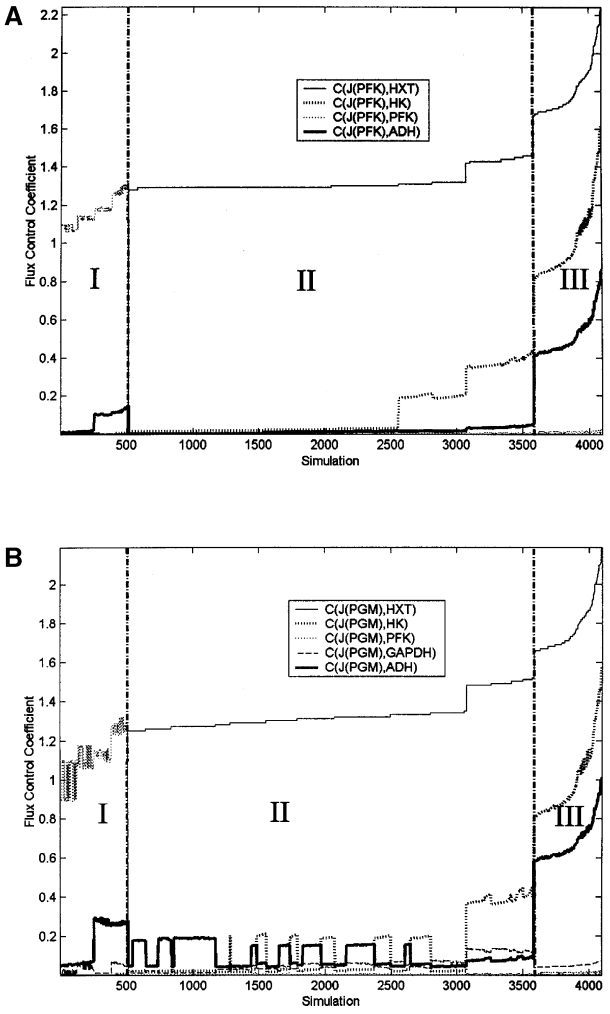


**Fig. 4. Plots of flux control coefficients for (A) upper and (B) lower glycolytic enzymes against simulation number.** The control regimes are divided into the three main groups I, II and III, and further subdivided by the level of secondary flux control exerted by each enzyme. PFK has dominating control under regime I, while HXT has dominating control under regimes II and III. Regime III can be distinguished from regime II by the significant flux control exerted by ADH.

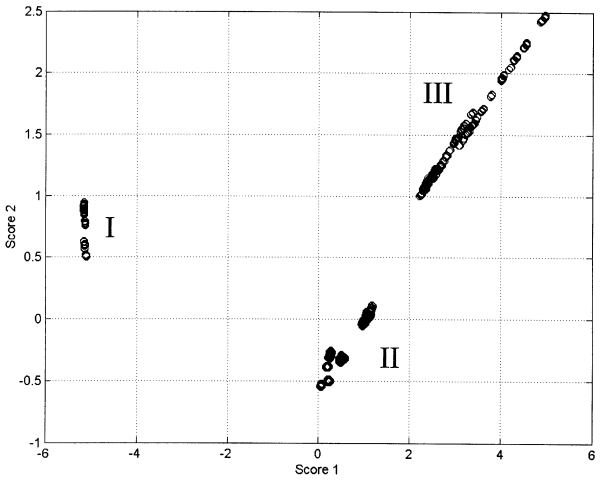


**Fig. 5. Score plot for PCA of the flux control coefficients for all steps in all the models resulting from parameter scanning (see text).** The labelled clusters are readily distinguished correspond to flux control regimes I, II and III in Fig. 4. Subdivision of the major clusters as shown in Fig. 4 can also be seen in this plot.

employed a stochastic fitting procedure to estimate optimal values for the $V_{max}$ values of the glycolytic steps. This procedure attempts to minimize the difference between the model and an experimental steady state and, though an exact fit was not obtained, several close fits were. This approach possesses the twin advantages of simultaneously fitting all steps in the model, and providing a population of candidate fits that, if the fitness landscape of the model resembles that of the experimental system, may itself be considered to describe the population of the experimental system.

Although kinetic parameters ($K_m$, $K_{eq}$, $k_{cat}$, etc.) of each step were used in the fitting procedure of [7], we chose not to employ them as parameters for evolutionary optimization in this paper in order to avoid underdetermination. We were initially concerned that in ignoring kinetic parameters for fitting, we could be ignoring critical factors for model performance. However, other work suggests that the important control properties of biochemical pathways are quite robust to small changes in the kinetic parameters of their constituent enzymes [29], consistent with the expectations of metabolic control analysis [30]. This would seem to imply that the differences in $K_m$ between the determined and *in vivo* values for the model enzymes, except where large, are of only minor importance. Furthermore the values of kinetic constants over a series of experiments are usually consistent, and the error over all experiments can be much greater than that seen in any single experiment [31]. We therefore reasoned that, for the fitting procedure, there was little need to account for the experimental error in the evaluation of Michaelis constants. We thus considered that, for fitting the model, the best representation of the likely origins of the difference between *in vivo* and *in vitro* performance of individual enzymes was the difference between the effective enzyme activities as described by $V_{max}$.

The failure of the fitting procedure to match *in vivo* performance may be problematic, but we believe the results still to be of value. Experimental values of metabolite concentration and flux are obtained from populations of yeast cells and so reflect an aggregate of the states of many individual organisms. Although no fitted model in this paper individually replicates the *in vivo* glycolytic system investigated in [7] exactly, it is arguable whether the majority of yeast cells (as represented by the model of glycolysis) in the studied cultures would correspond to the experimental results either [32,33]. Systematic variations within such a population are of interest because they may reveal certain global characteristics of the system, such as unified or distributed coresponse to perturbation. Linkage between the responses of subgroups of enzymes in the pathway can provide useful information for metabolic engineering, in terms of which steps are 'lumped' together, and so respond as a unit [34]. For the fitting experiments described herein, perturbations to the system are made through varying *in silico* the expression levels of these enzymes; thus linkage between control coefficients might imply a physiological

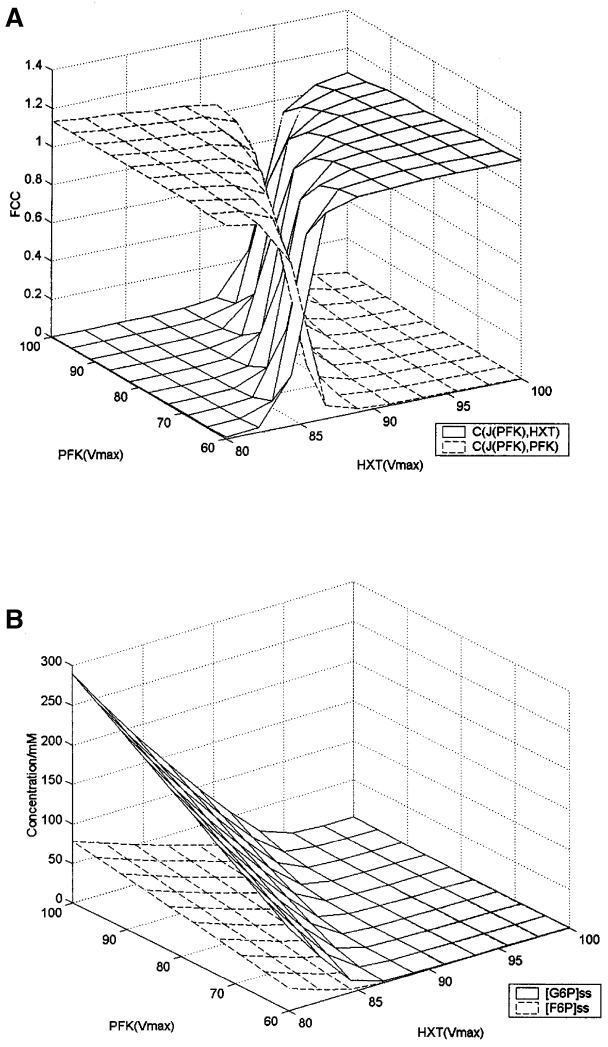


**Fig. 6. A plot of $C^{PFK}_{HXT}$ and $C^{PFK}_{PFK}$ against limiting rates for hexose transport and PFK, illustrating the switch between PFK and HXT-dominated flux control regimes.** PFK control derives from a reduction in limiting rate for PFK at high levels of glucose flux across the membrane. A plot corresponding to the same region of parameter space in HXT and PFK limiting rate, illustrating the internal steady-state concentrations of glucose-6-phosphate and fructose-6-phosphate. The concentrations of both these metabolites can be seen to rise rapidly as the system enters PFK control. The concentration of G6P in particular rises quickly to pathological levels (> 100 mM).

method of controlling glycolytic response achievable by coordinated regulation of enzyme expression.

## Control of glycolytic flux in the model systems

All the models that were fitted to *in vivo* steady-state metabolite concentration were found to operate under a single regime for glycolytic flux control, in which hexose transport has more-or-less complete control of flux, with a secondary role for hexokinase and the remainder of main-chain glycolysis having only minimal relevance. This pattern has previously been observed in a study of glycolytic flux control in rat heart perfused with glucose [35]. PFK, which has traditionally been considered the 'key' enzyme in the control of glycolysis [2,36,37], was seen to play no significant role in terms of flux control in these models.

Flux-control coefficients represent the extent to which the flux through one step of a pathway responds to a change in flux through another step [21]. For variations in enzyme limiting rates, correlations between FCCs may reveal whether the control of pathway flux through a step operates under only one, or one of several rival schemes depending on the precise pattern of enzyme expression. The correlations observed in this study suggest that the flux control is partitioned between HXT and a coherent unit of flux control formed from main chain glycolysis and the branching steps. As the control exerted by the hexose transport step on fluxes through the rest of glycolysis increases, the combined flux control by the branching steps and by the main-chain glycolytic enzymes is relaxed.

Even though there is some partitioning of flux control between sections of yeast glycolysis, and a (potentially unreachable) region of parameter space in which PFK dominates flux control it is clear that, at least in these models, hexose transport can be considered to be a 'pace making' step for glycolysis under a wide range of conditions. This role for hexose transport is not a new proposal, and this property of the glycolysis pathway has been observed in other models [4,38]. Neither HXT nor HK is insensitive to the levels of its own product, and therefore the glycolytic pathway is not a 'slave' pathway to either of those steps [39].

*S. cerevisiae* possesses 20 genes that encode proteins homologous to HXTs, though not all of them are transporters, nor are they all specific for glucose [39–41]. The variety of transporters not only allows the organism to grow on substrates other than glucose, but it also provides for at least two modes of glucose uptake: a high-affinity mode that operates at low glucose concentrations and a low-affinity mode that is used when the environmental glucose concentration rises. The membrane-spanning transporters operate by facilitated diffusion, but they are not constitutively expressed for either affinity mode. Instead, the transporters are transcriptionally regulated by at least three known modes of induction, which operate in different combinations dependent on the prevailing concentration of glucose [40]. Hexose transport is thus expected to take an active role in the regulation of glycolytic flux, and evolutionary selection for the intricate control of function and regulation observed in its hexose transport system [39,40,42,43] appears to be aimed at regulating glycolysis and ATP supply.

Glucose is also known to regulate gene expression, facilitating its own use by inducing expression of genes for its own metabolism and repressing those involved in processing other carbon sources [44]. It has been postulated that there are multiple such regulatory systems, some direct, and some indirectly operating through glucose-dependent cues [41]. It has also been noted that there is a more-or-less linear relationship between regulation of glucose transport capacity in *S. cerevisiae* and residual substrate concentration in chemostat cultures [45]. It was noted in the same study that at low dilution rates (i.e. low glucose levels) where the high affinity transport system dominates, the relationship breaks down such that HK activity is constant. This has the implication that the high affinity glucose transport system (unlike the low affinity system) acts so as to maintain a constant intracellular supply of glucose, and constant

glycolytic flux in the face of near-starvation. The hexose transport system here appears to behave in such a manner as to maintain glucose flux across the membrane at a higher level than would otherwise be expected [45,46].

Hexose transport has been shown to exert the bulk of control over growth rate and glucose repression in mutant yeast expressing only the HXT7 (high-affinity) glucose transporter [47], and over the frequency of glycolytic oscillations in yeast [48]. This latter set of experiments extends observations of HXT control over glycolytic flux to nonsteady state systems. Hexose transport has also been shown to be the major flux-control step in *S. bayanus* glycolytic flux control [49]. The evolutionary effort required to develop and maintain this set of biological checks and balances is intuitively indicative of some importance to maintaining consistent rates of glucose transport, which is in line with the observation in these models that control of glycolytic flux under normal operating conditions is strongly dependent on glucose transport flux. The minor role played by glycolytic enzymes in the control of glycolytic flux observed here is also consistent with previous observations.

Regime I (Figs 4 and 5), in which PFK is the dominant control step, is of particular interest given the historical importance placed on PFK as a 'rate-limiting' enzyme in yeast glycolysis [2,36,37]. For this model, majority control of glycolytic flux passes from hexose transport to PFK for a given glucose influx when the limiting rate through PFK falls (Fig. 6A). As has been previously suggested, this effect could derive from such causes as allosteric regulation or reduced expression level [37,50]. However, reduction of PFK($V_{max}$) results in the accumulation of what would be expected to be pathological levels of Glc6*P* and Fru6*P* (Fig. 6B), reminiscent of the proposed effect of removing the glycosomal membrane from trypanosomes [11]. However, for this restrictive model of glucose-derepressed yeast glycolysis the fluxes to glycogen and trehalose have been set at constant values, and so the alternative routes for disposal of these intermediates are somewhat less flexible than might be expected *in vivo*.

It has been suggested that this model may represent the *Tps1*Δ phenotype, in which the trehalose phosphate synthase activity that may limit hexokinase (reducing glucose uptake) is not present [7]. This is also suggested by the results of our parameter scanning, where only 12.5% of systems with increased HXT($V_{max}$) reach steady-state. Those systems with increased HXT limiting rate that are able to reach steady-state share the characteristics of reduced HK($V_{max}$), consistent with feedback from trehalose 6-phosphate to HKs (absent in this model). Steady-state is recovered in some model scans by a reduced limiting rate for PFK, but increased ALD($V_{max}$). The pathological effect of accumulating Fru6*P* and Glc6*P* may well be alleviated by different mechanisms *in vivo*, but for the purposes of this model of glucose-derepressed yeast glycolysis the PFK control region is rendered unreachable.

Fivefold overexpression of PFK in *S. cerevisiae* was also previously seen not to increase glycolytic flux under anaerobic conditions, the conditions of the studied model [51]. Likewise, regulation of PFK by Fru2,6$P_2$ does not seem to affect glycolytic flux to any great extent, despite the implications of models that place PFK central to control of glycolysis [52,53]. Over-expression of other enzymes in the pathway, both individually and in various combinations, has also been seen to have little or no effect on glycolytic flux, concordant with this model [54].

## CONCLUSIONS

Yeast glycolysis is one of a very few metabolic systems for which comprehensive kinetic data are available. Such complex, highly integrated systems are difficult and expensive to elucidate by laboratory experiment, and their future interpretation and analysis will rest heavily on the use of computational and bioinformatics techniques. We employed some of these techniques to investigate patterns of flux control in *S. cerevisiae* glycolysis. Recent experimental work suggests that control of glycolytic flux in *S. cerevisiae* resides mostly in the transmembrane glucose transport step under a wide range of conditions, although a role has previously been suggested for flux control by PFK. We used parameter scanning of a detailed model of glucose-derepressed yeast glycolysis, fitted to experimental data, in order to simulate a much wider scope of variation in enzyme expression levels than could reasonably be carried out *in vitro* or *in vivo*. Our results suggest that, over a wide range of operational parameters, control of the glycolytic flux may be classified into three major regimes, one of which is dominated by PFK flux control but is perhaps biologically unfeasible, while the two accessible control regimes operate under majority hexose transport flux control.

## ACKNOWLEDGEMENTS

The authors would like to thank Bas Teusink for supplying the SCAMP model of yeast glycolysis, David Broadhurst for HOBBES and statistical advice, and the referees for their helpful and improving suggestions.

## REFERENCES

1. Dandekar, T., Schuster, S., Snel, B., Huynen, M. & Bork, P. (1999) Pathway alignment: application to the comparative analysis of glycolytic enzymes. *Biochem. J.* **343**, 115–124.
2. Boiteux, A. & Hess, B. (1981) Design of glycolysis. *Phil. Trans. Roy. Soc. Lond. B.* **293**, 5–22.
3. Eschrich, K., Schellenberger, W. & Hofmann, E. (1990) A hysteretic cycle in glucose-6-phosphate metabolism observed in a cell-free yeast extract. *Eur. J. Biochem.* **188**, 697–703.
4. Cortassa, S. & Aon, M.A. (1997) Distributed control of the glycolytic flux in wild-type cells and catabolite repression mutants of Saccharomyces cerevisiae growing in carbon-limited chemostat cultures. *Enzyme Microbial Technol.* **16**, 761–770.
5. Rizzi, M., Baltes, M., Theobald, U. & Reuss, M. (1997) In vivo analysis of metabolic dynamics in *Saccharomyces cerevisiae* 2. Mathematical model. *Biotechnol. Bioengineering* **55**, 592–608.
6. Bier, M., Bakker, B.M. & Westerhoff, H.V. (2000) How yeast cells synchronize their glycolytic oscillations: a perturbation analytic treatment. *Biophys. J.* **78**, 1087–1093.
7. Teusink, B., Passarge, J., Reijenga, C.A., Esgalhado, E., van der Weijden, C.C., Schepper, M., Walsh, M.C., Bakker, B.M., van Dam, K., Westerhoff, H.V. & Snoep, J.L. (2000) Can yeast glycolysis be understood in terms of in vitro kinetics of the constituent enzymes? Testing biochemistry. *Eur. J. Biochem.* **267**, 5313–5329.
8. Wolf, J. & Heinrich, R. (2000) Effect of cellular interaction on glycolytic oscillations in yeast: a theoretical investigation. *Biochem. J.* **345**, 321–334.
9. Bakker, B.M., Walsh, M.C., terKuile, B.H., Mensonides, F.I.C., Michels, P.A.M., Opperdoes, F.R. & Westerhoff, H.V. (1999)

Contribution of glucose transport to the control of the glycolytic flux in *Trypanosoma brucei*. *Proc. Natl Acad. Sci. USA* **96**, 10098–10103.
10. Bakker, B.M., Michels, P.A.M., Opperdoes, F.R. & Westerhoff, H.V. (1999) What controls glycolysis in bloodstream form *Trypanosoma brucei*? *J. Biol. Chem.* **274**, 14551–14559.
11. Bakker, B.N., Mensonides, F.I.C., Teusink, B., vanHoek, P., Michels, P.A.M. & Westerhoff, H.V. (2000) Compartmentation protects trypanosomes from the dangerous design of glycolysis. *Proc. Natl Acad. Sci. of the USA* **97**, 2087–2092.
12. Bakker, B.M., Westerhoff, H.V., Opperdoes, F.R. & Michels, P.A.M. (2000) Metabolic control analysis of glycolysis in trypanosomes as an approach to improve selectivity and effectiveness of drugs. *Mol. Biochem. Parasitol.* **106**, 1–10.
13. Giersch, C. (2000) Mathematical modelling of metabolism. *Curr. Opin. Plant Biol.* **3**, 249–253.
14. Mendes, P. (1993) Gepasi – a software package for modelling the dynamics, steady-states and control of biochemical and other systems. *Comput. Applicat. Biosci.* **9**, 563–571.
15. Mendes, P. (1997) Biochemistry by numbers: simulation of biochemical pathways with Gepasi 3. *Trends Biochem. Sci.* **22**, 361–363.
16. Mendes, P. & Kell, D.B. (1998) Non-linear optimization of biochemical pathways: applications to metabolic engineering and parameter estimation. *Bioinformatics* **14**, 869–883.
17. Kell, D.B. & Mendes, P. (2000) Snapshots of systems: metabolic control analysis and biotechnology in the post-genomic era. *Technological and Medical Implications of Metabolic Control. Analysis* (Cornish-Bowden, A.J. & Cardenas, M.L., eds), pp. 3–25. Kluwer Academic, Amsterdam.
18. Kacser, H. & Burns, J.A. (1973) The control of flux. *Symposia Soc. Exp. Biol.* **27**, 65–104.
19. Kacser, H., Burns, J.A. & Fell, D.A. (1995) The control of flux. *Biochem. Soc. Trans.* **23**, 341–366.
20. Heinrich, R. & Schuster, S. (1996) *The Regulation of Cellular Systems*. Chapman & Hall, New York.
21. Fell, D.A. (1997) *Understanding the Control of Metabolism*, Portland, London.
22. Weiss, N.A. & Hassett, M.J. (1991) *Introductory Statistics*. Addison-Wesley, Reading, MA.
23. Press, W.H., Teukolsky, S.A., Vetterling, W.T. & Flannery, B.P. (1992) *Numerical Recipes in C, the Art of Scientific Computing*, 2nd edn. Cambridge University Press, Cambridge, UK.
24. Otto, M. (1999) *Chemometrics: Statistics and Computer Application in Analytical Chemistry*. Wiley-VCH, Weinhein.
25. Martens, H. & Naes, T. (1989) *Multivariate Calibration*. John Wiley, Chichester.
26. Joliffe, L.T. (1986) *Principal Component Analysis*. Springer-Verlag, New York.
27. Shaw, A.D., Winson, M.K., Woodward, A.M., McGovern, A., Davey, H.M., Kaderbhai, N., Broadhurst, D.I., Gilbert, R.J., Taylor, J., Timmins, E.M., Alsberg, B.K., Rowland, J.J., Goodacre, R. & Kell, D.B. (1999) Rapid analysis of high-dimensional bioprocesses using multivariate spectroscopies and advanced chemometrics. *Adv. Biochem. Bioengineering* **66**, 83–113.
28. Jones, A., Shaw, A.D., Salter, G.J., Bianchi, G. & Kell, D.B. (1998) The exploitation of chemometric methods in the analysis of spectroscopic data: application to olive oils. In *Lipid Analysis of Oils and Fats* (Hamilton, R.J., ed.), Chapman & Hall, London.
29. Barkai, N. & Leibler, S. (1997) Robustness in simple biochemical networks. *Nature* **387**, 913–917.
30. Kell, D.B. (1999) Revolutionary Ideas Come Round Again [letter]. *Nature* **397**, 644.
31. Duggleby, R.G. (1991) Analysis of biochemical data by nonlinear regression: is it a waste of time? *Trends Biochem. Sci.* **16**, 51–52.
32. Davey, H.M. & Kell, D.B. (1996) Flow cytometry and cell sorting of heterogeneous microbial populations: the importance of single-cell analysis. *Microbiol. Rev.* **60**, 641–696.
33. Kell, D.B., Ryder, H.M., Kaprelyants, A.S. & Westerhoff, H.V. (1991) Quantifying heterogeneity: flow cytometry of bacterial cultures. *Antonie van Leeuwenhoek* **60**, 145–148.
34. Raamsdonk, L.M., Teusink, B., Broadhurst, D., Zhang, N., Hayes, A., Walsh, M.C., Berden, J.A., Brindle, K.M., Kell, D.B. & Rowland, J.J. (2001) A functional genomics strategy that uses metabolome data to reveal the phenotype of silent mutations. *Nat. Biotechnol.* **19**, 45–50.
35. Kashiwaya, Y., Sato, K., Tsuchiya, N., Thomas, S., Fell, D.A., Veech, R.L. & Passonneau, J.V. (1994) Control of glucose utilization in working perfused rat-heart. *J. Biol. Chem.* **269**, 25502–25514.
36. Stryer, L. (1995) *Biochemistry (Fourth Edition)*. W.H. Freeman, New York.
37. Evans, P.R., Farrants, G.W. & Hudson, P.J. (1981) Phosphofructokinase: structure and control. *Phil. Trans. Roy. Soc. Lond. B.* **293**, 53–62.
38. Gancedo, C. & Serrano, R. (1989) Energy-yielding metabolism. In *The Yeasts*, 2nd edn. (Harrison, J.S., ed.), pp. 205–259. Academic Press, London.
39. Teusink, B. & Westerhoff, H.V. (2000) 'Slave' metabolites and enzymes – a rapid way of delineating metabolic control, *Eur. J. Biochem.* **267**, 1889–1893.
40. Ozcan, S. & Johnston, K. (1999) Function and regulation of yeast hexose transporters. *Microbiol. Mol. Biol. Rev.* **63**, 554–569.
41. Vaulont, S., Vasseur-Cognet, M. & Kahn, A. (2000) Glucose regulation of gene transcription. *J. Biol. Chem.* **275**, 31555–31558.
42. Ciriacy, M. & Reifenberger, E. (1997) Hexose transport. In *Yeast Sugar Metabolism: Biochemistry, Genetics, Biotechnology and Applications* (Entian, K.-D., ed.), pp. 45–65. Technomic, Lancaster.
43. Reifenberger, E., Boles, E. & Ciriacy, M. (1995) Identification of novel HXT genes in *Saccharomyces cerevisiae* reveals the impact of individual hexose transporters on the glycolytic flux. *Mol. Microbiol.* **16**, 157–167.
44. Johnston, M. (1999) Feasting, fasting and fermenting – glucose sensing in yeast and other cells. *Trends Genet.* **15**, 29–33.
45. Postma, E., Scheffers, W.A. & van Dijken, J.P. (1989) Kinetics of growth and glucose transport in glucose-limited chemostat cultures of *Saccharomyces cerevisiae* CBS 8066. *Yeast* **5**, 159–165.
46. Walsh, M.C., Smits, H.P., Scholte, M. & Van Dam, K. (1994) Affinity of glucose transport in *Saccharomyces cerevisiae* is modulated during growth on glucose. *J. Bacteriol.* **176**, 953.
47. Ye, L., Kruckeberg, A.L., Berden, J.A. & Van Dam, K. (1999) Growth and glucose repression are controlled by glucose transport in *Saccharomyces cerevisiae* cells containing only one glucose transporter. *J. Bacteriol.* **181**, 4673–4675.
48. Reijenga, K.A., Snoep, J.L., Diderich, J.A., van Verseveld, H.W., Westerhoff, H.V. & Teusink, B. (2001) Control of glycolytic dynamics by hexose transport in *Saccharomyces cerevisiae*. *Biophys. J.* **80**, 626–634.
49. Diderich, J.A., Teusink, B., Valkier, J., Anjos, J., SpencerMartins, I., vanDam, K. & Walsh, M.C. (1999) Strategies to determine the extent of control exerted by glucose transport on glycolytic flux in the yeast Saccharomyces bayanus. *Microbiology-UK.* **145**, 3447–3454.
50. Kopperschlager, G. & Heinisch, J. (1997) Phosphofructokinase. In *Yeast Sugar Metabolism: Biochemistry, Genetics, Biotechnology and Applications* (Entian, K.-D., ed.), pp. 97–118. Technomic, Lancaster.
51. Davies, S.E.C. & Brindle, K.M. (1992) Effects of overexpression of phosphofructokinase on glycolysis in the yeast *Saccharomyces cerevisiae*. *Biochemistry* **31**, 4729–4735.

52. Muller, S., Zimmermann, F.K. & Boles, E. (1997) Mutant studies of phosphofructo-2-kinase do not reveal an essential role of fructose-2,6-biphosphate in the regulation of carbon fluxes in yeast cells. *Microbiology* **143**, 3055–3061.
53. Goncalves, P. & Planta, R.J. (1998) Starting up yeast glycolysis. *Trends Microbiol.* **6**, 314–319.
54. Schaaf, I., Heinisch, J. & Zimmermann, F.K. (1989) Overproduction of glycolytic enzymes in yeast. *Yeast* **5**, 285–290.

## APPENDIX 1: DIFFERENTIAL EQUATIONS

The set of ordinary differential equations that describes time-dependence of the metabolite concentrations is given below. This set differs from that in [7] in that it includes explicit equations for adenosine phosphate and triose phosphate species (A5, A6, A13–A15), and in that there is no involvement of the adenosine species in the succinate branch. Enzyme kinetics are as described previously [7].

$$\frac{d[GLC_i]}{dt} = \nu HXT - \nu HK \quad (A1)$$

$$\frac{d[Glc6P]}{dt} = \nu HK - \nu PGI - \nu glycogen - 2 \times \nu trehalose \quad (A2)$$

$$\frac{d[Fru6P]}{dt} = \nu PGI - \nu PFK \quad (A3)$$

$$\frac{d[Fru1,6P_2]}{dt} = \nu PFK - \nu ALD \quad (A4)$$

$$\frac{d[\text{glycerone phosphate}]}{dt} = \nu ALD - \nu TPI - \nu Gro3PDH \quad (A5)$$

$$\frac{d[\text{glycerone phosphate}]}{dt} = \nu ALD + \nu TPI - \nu Gra3PDH \quad (A6)$$

$$\frac{d[Gri1,3P_2]}{dt} = \nu Gra3PDH - \nu PGK \quad (A7)$$

$$\frac{d[Gri3P]}{dt} = \nu PGK - \nu PGM \quad (A8)$$

$$\frac{d[Gri2P]}{dt} = \nu PGM - \nu ENO \quad (A9)$$

$$\frac{d[\text{phospho}\textit{enol}\text{pyruvate}]}{dt} = \nu ENO - \nu PYK \quad (A10)$$

$$\frac{d[\text{pyruvate}]}{dt} = \nu PYK - \nu PDC \quad (A11)$$

$$\frac{d[\text{acetaldehyde}]}{dt} = \nu PDC - \nu ADH - \nu succinate \quad (A12)$$

$$\frac{d[AMP]}{dt} = \nu AK \quad (A13)$$

$$\frac{d[ADP]}{dt} = \nu HK + \nu ATPase + \nu glycogen + \nu trehalose + \nu PFK - \nu PGK - \nu PYK - 2 \times \nu AK \quad (A14)$$

$$\frac{d[ATP]}{dt} = \nu PGK + \nu PYK + \nu AK - \nu HK - \nu glycogen - \nu trehalose - \nu PFK - \nu ATPase \quad (A15)$$

$$\frac{d[NAD]}{dt} = \nu glycerol + \nu ADH - 3 \times \nu succinate - \nu Gra3PDH \quad (A16)$$

$$\frac{d[NADH]}{dt} = \nu Gra3PDH + 3 \times \nu succinate - \nu Gro3PDH - \nu ADH \quad (A17)$$

## APPENDIX 2: DEVIATION FROM THE TEUSINK *ET AL.* MODEL

Variations between the model used for this work and the model published in [7].

The variant parameters for enzyme rate equations are those that were supplied to us in the model made available by one of the authors of [7], and the only significant difference between the performance of our model and that in [7] is the value for steady state pyruvate concentration (Table A1).

**Table A1. Differences between the current model and that in Teusink *et al.* [7].** Minor differences between this paper and [7] in values of kinetic parameters for the model are listed. The only significant difference in model performance is the steady-state concentration of pyruvate, which in both cases is over four times as large as the reported experimental concentration.

| Item | Teusink *et al.* (2000) [7] | This paper |
|---|---|---|
| $K_{eq}$(ADH) | $1.45 \times 10^4$ | $6.9 \times 10^{-5}$ |
| $K_{eq}$(PGI) | 0.314 | 0.29 |
| $k_{ATPase}$ | 33.7 | 39.5 |
| $K_m$P2G(PGM) | 0.1 | 0.08 |
| cGra3*P*DH | Not given | 1.0 |
| $K_i$NAD(ADH) | 0.92 | Not used |
| cFru6*P*(PFK) | 0 | Not used |
| gT(PFK) | 1 | Not used |
| $[pyruvate]_{ss}$ | 8.52 | 8.37 |